

Field-induced partial disorder in a Shastry-Sutherland lattice

Received: 5 October 2022

Accepted: 13 June 2023

Published online: 19 June 2023

Madalynn Marshall¹, Brianna R. Billingsley², Xiaojian Bai^{1,3}, Qianli Ma¹,
Tai Kong^{1,2,4} & Huibo Cao¹✉

A 2-Q antiferromagnetic order of the ferromagnetic dimers was found below $T_N = 2.9$ K in the Shastry-Sutherland lattice $\text{BaNd}_2\text{ZnS}_5$ by single crystal neutron diffraction. The magnetic order can be understood by the orthogonal arrangement of local Ising Nd spins, identified by polarized neutrons. A field was applied along $[1\ -1\ 0]$ to probe the observed metamagnetic transition in the magnetization measurement. The field decouples two magnetic sublattices corresponding to the propagation vectors $\mathbf{q}_1 = (\frac{1}{2}, \frac{1}{2}, 0)$ and $\mathbf{q}_2 = (-\frac{1}{2}, \frac{1}{2}, 0)$, respectively. Each sublattice shows a “stripe” order with a Néel-type arrangement in each single layer. The “stripe” order with \mathbf{q}_1 remains nearly intact up to 6 T, while the other one with \mathbf{q}_2 is suppressed at a critical field $H_c \sim 1.7$ T, indicating a partial disorder. The H_c varies with temperature and is manifested in the H - T phase diagram constructed by measuring the magnetization in $\text{BaNd}_2\text{ZnS}_5$.

Exotic non-trivial magnetic behavior has emerged in magnetic systems with geometrical frustration. The kagome and triangular lattices are common examples of two-dimensional (2D) frustrated lattices^{1,2}. More elusive is the 2D orthogonal dimer lattice famously realized in the material $\text{SrCu}_2(\text{BO}_3)_2$ ^{3,4}, which has been discovered to host a quantum spin liquid phase^{5–8}. This lattice can be described by the Shastry-Sutherland (SS) model which consists of a 2D orthogonal arrangement of the spin dimers where the ratio between the two magnetic interactions, $\delta = J/J'$ with J and J' as the antiferromagnetic inter- and intra-dimer interactions, respectively, is critical for controlling magnetic states in the Shastry-Sutherland lattice (SSL)⁹. The δ ratio of 0.675 and 0.765 separate the dimer singlet, plaquette singlet and Néel phase, respectively, in the phase diagram of the SS model^{10,11}.

Resultantly, rich magnetic phase diagrams have been constructed for SSL materials from the field-induced evolution of the magnetic order. One common feature are fractionalized magnetization plateaus, which likely originate from the transition of a dimer singlet ground state to the formation of superstructures of the field-induced triplet dimers such as in $\text{SrCu}_2(\text{BO}_3)_2$ ^{10,12–21}. The SSL is also found in families such as the rare earth tetraborides RB_4 (R = rare earth)^{22–24}, BaR_2TO_5 (R = rare earth, T = transition metal)^{25–28}, $\text{R}_2\text{T}_2\text{In}$ (R = rare earth, T =

transition metal)^{29–31} and $\text{RE}_2\text{Pt}_2\text{Pb}$ (R = rare earth)³². The magnetic ordered states can vary significantly from the insulator $\text{SrCu}_2(\text{BO}_3)_2$ which possesses a Heisenberg type exchange interaction to the metallic RB_4 family where a Ruderman-Kittel Kasuya-Yosida (RKKY) type interaction is observed between the moments giving it a long-range order and possessing Ising-like moments oriented perpendicular to the SSL planes^{33–35}. However, SSL materials such as $\text{Yb}_2\text{Pt}_2\text{Pb}$ ^{32,36–39}, have been found to exhibit field-induced metamagnetic transitions associated with partially disordered states, where at low temperatures a Luttinger liquid state has been realized.

Consequently, only very few SSL materials were reported to possess ferromagnetic dimers, including the insulator $\text{BaNd}_2\text{ZnO}_5$ ²⁵ and metallic TmB_4 ^{23,34,40}. Considering the newly explored BaR_2TO_5 family, although it is chemically diverse, the formation of the SSL will only occur for the lighter rare earth elements and successful single crystal growth has not been reported. The sulfide counterpart, BaR_2TS_5 , which crystallizes into the same space group ($I4/mcm$) as the SSL BaR_2TO_5 materials, remains largely unexplored and recently large single crystals of $\text{BaNd}_2\text{ZnS}_5$ ^{41,42} have been synthesized exhibiting a $T_N = 2.9$ K. The dimers of the SSL in $\text{BaNd}_2\text{ZnS}_5$ are formed by the Nd atoms having inter-dimer lengths of 4.151 Å and intra-dimer lengths of

¹Neutron Scattering Division, Oak Ridge National Laboratory, Oak Ridge, TN 37831, USA. ²Department of Physics, University of Arizona, Tucson, AZ 85721, USA.

³Department of Physics and Astronomy, University of Louisiana, Baton Rouge, LO 70803, USA. ⁴Department of Chemistry and Biochemistry, University of Arizona, Tucson, AZ 85721, USA. ✉e-mail: caoh@ornl.gov

3.596 Å. A metamagnetic transition is observed in the $M(H)$ with \mathbf{H} along $[1 \bar{1} 0]$, indicating this SSL material an excellent candidate for studying the intricate dimer physics from the field-induced magnetic phase evolution.

In this work, we report a 2-Q magnetic order in the SSL $\text{BaNd}_2\text{ZnS}_5$, determined by single crystal neutron diffraction. We utilize polarized neutrons to provide insight into the local magnetic anisotropy of the Nd spins and reveal the origin of the 2-Q magnetic order. The resulting field-induced evolution of the magnetic phases were characterized by magnetization measurements with the critical input from single crystal neutron diffraction. A partially disordered dimer liquid state was found and a “spin-flip-or-flop” mechanism was proposed to describe the dimer liquid state.

Results and discussions

Zero field magnetic structure

$\text{BaNd}_2\text{ZnS}_5$ exhibits 2D SSL layers of magnetic Nd^{3+} ($J=9/2$) atoms separated by layers of Ba and Zn atoms and coordinated by S atoms. Nd^{3+} has a Kramers doublet ground state and behaves as a pseudospin $1/2$ ⁴³. Figure 1a, describes the Nd SSL where J' represents the intradimer interaction (nearest-neighbor) and J the interdimer interaction (next-nearest-neighbor), a typical SS interaction model. To understand the magnetic anisotropy of the Nd^{3+} spins in $\text{BaNd}_2\text{ZnS}_5$, we measured the local magnetic susceptibility tensor of the Nd^{3+} spins by polarized neutron diffraction^{44,45}. The local symmetry of the Nd atomic site, the $8h$ site of space group $I4/mcm$, implies the principal axes of the ellipsoid are along the $[1 \ 1 \ 0]$, $[1 \bar{1} \ 0]$ and $[0 \ 0 \ 1]$ directions. The bulk magnetic measurements have revealed the magnetic moments are easy in-plane⁴². Therefore, only one-field-direction along $[1 \bar{1} \ 0]$, was selected to detect the in-plane magnetic anisotropy of the Nd^{3+} spins. By measuring reflections in spin-up and spin-down neutron channels,

we obtained 17 good-quality flipping ratios to refine two free susceptibility tensor parameters in-plane. A suitable fitting of the flipping ratios could be reached, as shown by the Fig. 1b plot of the experimental versus calculated flipping ratios, using the software CrysPy. The in-plane principal axes of the Nd^{3+} magnetization ellipsoids, Fig. 1c, were found to be orthogonal to the dimer bond consistent with an Ising-spin nature with lengths $\chi_{//} = 0.183(22) \mu_B/T$ and $\chi_{\perp} = 0.033(22) \mu_B/T$. Similar to $\text{Yb}_2\text{Pt}_2\text{Pb}$ ³² the magnetic moments are found within the plane of the SSL and orthogonally arranged between two magnetic sublattices that satisfy the Ising behavior, contrary to that in $\text{SrCu}_2(\text{BO}_3)_2$ ¹⁴ and TmB_4 ²³. Instead of the well-known SSL interaction model, the resulting formation seemingly favors an effective square lattice magnetic model where J' and J'' are the potential interaction paths, as indicated by the orange line (i.e. the dimer bond) and the dashed black line, respectively, in Fig. 1f³². The symmetric terms of interaction J produce zero energy contribution due to the orthogonality of the spin arrangement between the neighboring orthogonal dimer bonds (shown in Fig. 1a as a standard SS spin model but ignored in Fig. 1f due to the zero-energy contribution from J for the Ising spins). While the antisymmetric terms of J in the spin Hamiltonian (see the full description in the SI) are likely weak as well, this will be shown by the field measurements presented later. Future inelastic neutron scattering measurements are needed to further confirm the interaction speculation here and interpret the spin dynamics in $\text{BaNd}_2\text{ZnS}_5$.

From the temperature-dependence of the magnetic scattering at $(\frac{1}{2} \ \frac{1}{2} \ 2)$, Fig. 1d, the magnetic order appears at ~ 3 K, consistent with the reported $T_N = 2.9$ K from the magnetic susceptibility measurements⁴². The solid red line in Fig. 1d, corresponds to the power law fitting of the intensity, $I - (T_N - T/T_N)^{2\beta}$, with a T_N reasonably fixed at 2.95 K, and a $\beta = 0.08(1)$ which is smaller than the expected $\beta = 1/8$ for a 2D Ising system³² and could be a result of the nature of the spin dimer

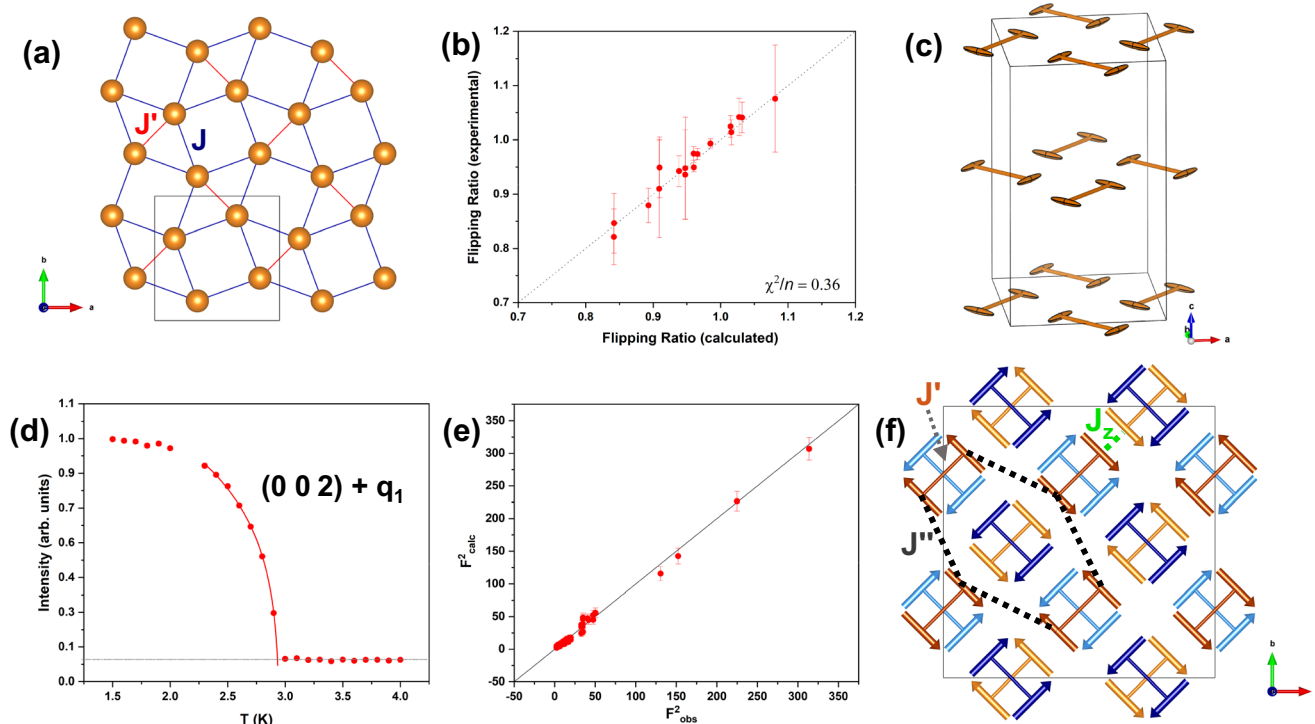


Fig. 1 | Zero-field magnetic structure refinement of $\text{BaNd}_2\text{ZnS}_5$. **a** SSL sublattice of Nd atoms in the ab plane. **b** Experimental versus calculated flipping ratio plot. **c** Local magnetic anisotropy of Nd dimers is shown by magnetic susceptibility tensors drawn as ellipsoids in unit cell of $\text{BaNd}_2\text{ZnS}_5$. **d** Temperature-dependent order parameter of peak $(\frac{1}{2} \ \frac{1}{2} \ 2)$, red line is the empirical power law fitting, $I - (T_m - T/T_m)^{2\beta}$. **e** Experimental versus

calculated structure factors at zero field. **f** 2-Q magnetic structure model for $\text{BaNd}_2\text{ZnS}_5$, the blue and orange represent the sublattices with $\mathbf{q}_1 = (\frac{1}{2}, \frac{1}{2}, 0)$ and $\mathbf{q}_2 = (-\frac{1}{2}, \frac{1}{2}, 0)$, respectively, and the light and dark color shades represent the different layers along the c axis. The J' and J'' interaction paths correspond to the dimer bond and the dashed black line, respectively. The J_z represents the nearest spin-spin interaction between layers.

lattice. As a product of the single crystal polarized neutron diffraction results, a suitable magnetic structure model could be immediately determined since the fit could be appropriately constrained with moments perpendicular to the dimer bonds. A 2- \mathbf{Q} AFM model consisting of two magnetic sublattices indexed by the propagation vectors $\mathbf{q}_1 = (\frac{1}{2}, \frac{1}{2}, 0)$ and $\mathbf{q}_2 = (-\frac{1}{2}, \frac{1}{2}, 0)$, resembling the AFM 2- \mathbf{Q} structure for $\text{BaNd}_2\text{ZnO}_5$ ²⁵ but with a different magnetic symmetry, best fit the zero-field data. The magnetic symmetry $P_{4/nnc}$ (#126.385) was then determined using the k-SUBGROUPSMAG program from the Bilbao Crystallographic server. Based on the body centered symmetry, the SSL layers are separated by a centering translation resulting in two inequivalent propagation vectors that each connects to one magnetic sublattice with a “stripe” order when viewing two layers together. Therefore, a FM interlayer interaction, J_z , also needs to be considered, which is likely as weak as J' due to the larger atomic distance between interacting spins, however, necessary to stabilize the magnetic order at zero field, distinct from the magnetic order reported in $\text{BaNd}_2\text{ZnO}_5$ ²⁵. Each SSL layer individually exhibits a Néel phase arrangement where the potential interaction paths consist of a dominant FM J' and a weak AFM J'' . The refined Nd magnetic moment was determined to be $2.6(1) \mu_B$. Figure 1e shows a plot of the calculated structure factor square (F^2_{calc}) versus the observed one (F^2_{obs}) and the magnetic structure can be seen in Fig. 1f where the orange and blue atoms represent the two different sublattices and the overlapping layers along the c axis are indicated by the light and dark color shades.

Field-induced phase evolution

The magnetization curves below T_N of $\text{BaNd}_2\text{ZnO}_5$ show kinks around 1.7 T for fields along the $[1 -1 0]$ direction, as shown by Fig. 2a, indicating a metamagnetic transition. To investigate this transition, single crystal neutron diffraction measurements were performed with an applied magnetic field of 2 and 6 T parallel to the $[1 -1 0]$ direction. As the field-induced transition emerges around 1.7 T, at 1.4 K, the field-

dependent magnetic scattering at $(1.5 \ 1.5 \ 1)$ disappears at 1.7 T (see Fig. 2c) signifying the stripe phase with $\mathbf{q}_2 = (-\frac{1}{2}, \frac{1}{2}, 0)$ is no longer present. Therefore, the kink shown in the magnetization measurement is a signature of the magnetic order-disorder transition in the magnetic sublattice with spins parallel to the field and the corresponding field can be viewed as the critical field H_C for this transition. For the other magnetic sublattice, the magnetic peak $(\frac{1}{2} \ \frac{1}{2} \ 4)$ gradually decreases with the field increasing but the majority of the magnetic peak signal is maintained up to 6 T (see Fig. 2c inset). By analyzing the neutron diffraction data collected at 2 and 6 T at 1.4 K, the refined magnetic moments for the stripe phase of the \mathbf{q}_1 magnetic sublattice with spins along $[1 \ 1 \ 0]$, perpendicular to the field direction, were determined to be $2.8(1)$ and $2.6(1) \mu_B$, respectively.

At 2 and 6 T the observed magnetic reflections from the diffraction patterns could be all indexed by $\mathbf{q}_1 = (\frac{1}{2}, \frac{1}{2}, 0)$, while no peaks could be indexed with $\mathbf{q}_2 = (-\frac{1}{2}, \frac{1}{2}, 0)$ when considering the body centering translation symmetry. Note, the body-centered unit cell is not a primitive cell and so \mathbf{q}_1 and \mathbf{q}_2 are not equivalent. From the k-SUBGROUPSMAG program, the low symmetry space group $P1$ (#1.1) was initially selected to test the potential magnetic models under field. The resulting refinement reveals a partially disordered state of ferromagnetic dimers at 2 T in one magnetic sublattice (Fig. 2e) and while the AFM order in the other magnetic sublattice with moments along $[1 \ 1 \ 0]$ (\mathbf{q}_1 magnetic sublattice) survives (Fig. 2e and 2f). The results also indicate the two magnetic sublattices are interaction-decoupled and can be separated under an applied field, which confirms that the interaction J between the two magnetic sublattices is weak, i.e., no strong antisymmetric exchange interactions between the orthogonally arranged neighboring Nd spin dimers. This separation can also be observed as two T_N 's connected to the two sublattices under field, see Supplementary Figs. S1 and S2. Considering the magnetic interaction distance and the localized f -electron feature for the rare-earth spins, both J' and J_z are much

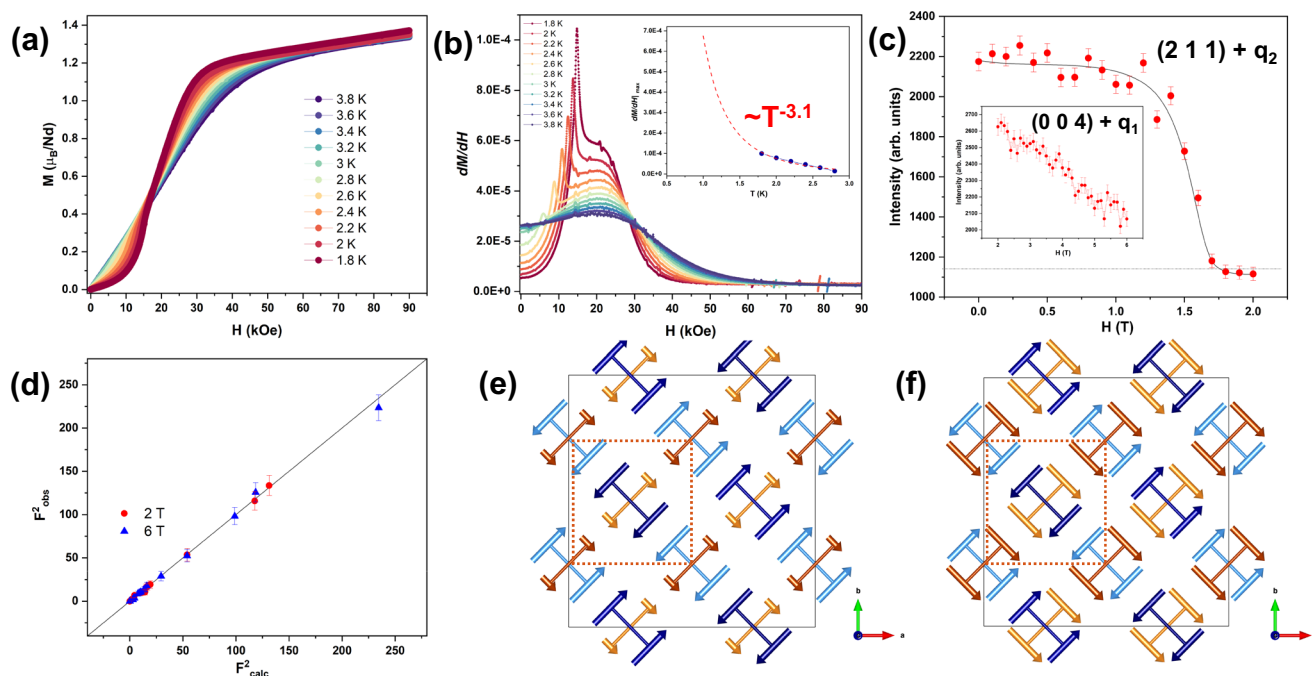


Fig. 2 | Field induced phase evolution and magnetic structure refinement at 2 and 6 T. **a** Magnetization measurement with $H/[1 -1 0]$ from 1.8 to 3.8 K. **b** Plots of dM/dH measured at constant temperature from 1.8 to 3.8 K, data were smoothed for the derivation, with an inset of dM/dH_{max} versus temperature as derived from the maximum value of the sharp peak in dM/dH , the red line represents the power-law dependence $-T^{-n}$ ($n = 3.1$). **c** Field-dependent order

parameter from 0 to 2 T at $(1.5 \ 1.5 \ 1)$. The inset for the field-dependent order parameter from 2 to 6 T at $(\frac{1}{2} \ \frac{1}{2} \ 4)$. **d** Experimental versus calculated structure factors at 2 T (red circles) and 6 T (blue triangles). **e** The refined magnetic structure of the partially disordered phase at 2 T and **f** the field polarized state at 6 T with the square lattice of FM spin dimers shown by the dashed dark orange lines.

weaker compared to the intra-dimer interaction J' . Therefore, the SSL in $\text{BaNd}_2\text{ZnS}_5$ can be viewed as two decoupled square lattices of ferromagnetic dimers that are loosely 3-dimensionally connected. While the magnetic phase transitions induced by the field up to 6 T along $[1 \bar{1} 0]$ at 1.4 K is likely only within the \mathbf{q}_2 magnetic sublattice with Nd^{3+} moments along $[1 \bar{1} 0]$. Therefore, the following discussions will be focused on only the magnetic dimer square sublattice with spins parallel to the field $[1 \bar{1} 0]$ (the square lattice of FM spin dimers is shown in Fig. 2e and f as the dark orange line for the magnetic sublattice with spins along $[1 \bar{1} 0]$).

Neutron diffraction revealed that the \mathbf{q}_2 stripe order is fully suppressed by the field at the critical field $H_C \sim 1.7$ T. Field-induced magnetic signal on top of the nuclear Bragg peaks were refined as uniformly aligned moments of $1.2(2) \mu_B$ at 2 T for the magnetic sublattice with the spin Ising axis along $[1 \bar{1} 0] // \mathbf{H}$, i.e., $0.6(1) \mu_B$ per Nd^{3+} if averaging it for the whole magnetic lattice, consistent with the increased magnetization in the bulk measurement. If we consider the model of the square lattice of ferromagnetic dimers as described above, each ferromagnetic dimer includes two parallel aligned spin-half moments and so makes a spin-1 dimer with $S=1$ as the ground state. When a field is applied, two kinds of dimer spin transitions among three magnetic components ($S_z = -1, 0, +1$) can occur and cause the order-disorder transition and yield the average induced moment as seen by neutrons. One is a spin-flip transition from $S_z = -1$ to $S_z = +1$ and the other one is a spin-flop transition from $S_z = -1$ to $S_z = 0$, the quantum version of the well-known spin-flop transition in a weak-magnetic-anisotropic AFM system^{46,47}. Both spin component transitions are illustrated in Fig. 3b. The flipped or flopped spin dimers are disordered in the lattice space because no additional superlattice ordering peaks were observed. Therefore, we refer to this partial disorder as a liquid-like state, i.e., dimer liquid. More dynamic measurements are needed to further characterize the nature of the dimer liquid state in contrast to the reported Luttinger liquid state in the SSL material $\text{Yb}_2\text{Pt}_2\text{Pb}^{48}$, the quantum spin liquid phase in the Kitaev honeycomb-lattice RuCl_3^{49} , and the magnetization plateau phases in the SSL material $\text{SrCu}_2(\text{BO}_3)_2^{10,12-21}$. At 6 T the square magnetic sublattice with Nd spins along $[1 \bar{1} 0]$ enters a field polarized state and has a refined magnetic moment of $2.8(1) \mu_B$, the magnetic structure is shown in Fig. 2f.

Phase diagram and spin dimer liquid

We can construct the field-temperature (H - T) phase diagram from the magnetization data upon varying temperature since neutron diffraction reveals that the kink observed in the magnetization indicates the disorder transition from the stripe order in the \mathbf{q}_2 magnetic sublattice. The critical field H_C at each temperature can be better observed as a sharp peak in the plots of dM/dH (see Fig. 2b), where upon cooling, the H_C shifts towards higher fields, $H_C \sim 1.5$ T at 1.8 K. Above H_C , the transition to the field polarized state can be seen by the broad bump feature at higher field. A contour plot mapping the values of dM/dH obtained from 1.8 to 3.8 K, is depicted in a H versus T (H - T) phase diagram describing the magnetic sublattice with spins parallel to the field direction $[1 \bar{1} 0]$, Fig. 3a, based on the bulk magnetization (circles) and susceptibility (diamonds and triangles) measurements under the field along $[1 \bar{1} 0]$ and neutron data (square). Phase I represents the 2-Q magnetically ordered stripe phase while phase II is the dimer liquid phase. The contour plot of dM/dH clearly defines the regions for Phase I and II and furthermore the transition to the field polarized state as Phase III. According to the neutron diffraction measurement at 1.4 K, no additional magnetic order was observed when the stripe phase enters the spin dimer liquid state, Phase II, at 1.7 T, indicating the critical region is further narrowed towards a possible critical point.

A similar temperature dependence of the behavior of H_C in Fig. 3a has been observed in the phase diagrams of geometrically frustrated lattices exhibiting field-induced quantum criticality, such as $\text{CoNb}_2\text{O}_6^{50,51}$ and RuCl_3^{49} , constructed from heat capacity measurements under field. A possible explanation of such a H - T behavior in $\text{BaNd}_2\text{ZnS}_5$ can be explained by field-melting the stripe ordered phase through “spin-flip-or-flop” transitions. The H - T phase diagram could also suggest the possibility that quantum criticality may exist in $\text{BaNd}_2\text{ZnS}_5$ at the lowest temperature. Additional evidence is shown by the plot of $dM/dH/\max$ versus T in the Fig. 2b inset that demonstrates the power law fitting $-T^n$, where it has been constrained to $n = 3.1$ to assess the possibility of quantum critical fluctuations as determined for the antiferromagnet CePtIn_4^{52} . Down to 1.8 K $\text{BaNd}_2\text{ZnS}_5$ resembles that of the linear higher temperature region in the power law fitting of CePtIn_4 , suggesting a certain similarity of the two systems. To explore these scenarios and reveal the enigmatic magnetic ground state of $\text{BaNd}_2\text{ZnS}_5$, low temperature heat capacity, magnetization and

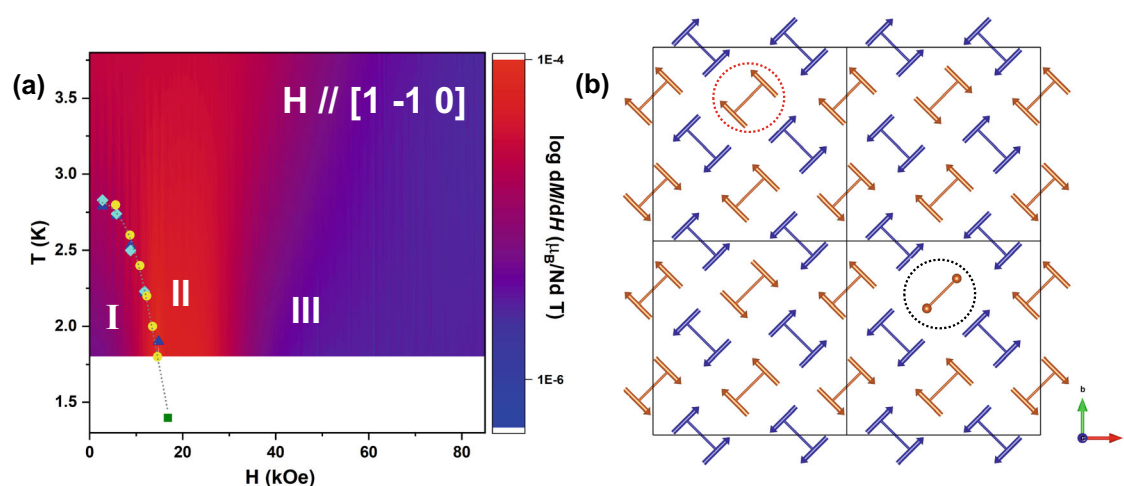


Fig. 3 | A constructed phase diagram along with possible dynamical magnetic patterns for disordered state. a Field versus T_N (H - T) phase diagram with $\mathbf{H} // [1 \bar{1} 0]$, the magnetic susceptibility, magnetization and neutron data are represented by the light blue diamonds and blue triangles for the two measurements which were performed, yellow circles and green squares, respectively. The H - T phase diagram overlays a contour plot mapping the values of

dM/dH obtained at constant temperatures, the values of dM/dH are represented by the color scale. **b** A possible dynamical magnetic pattern at the H_C , the dotted red-circle highlights the spin-flip transition from $S_z = -1$ to $S_z = +1$ and the dotted black-circle highlights the spin-flop transition from $S_z = -1$ to $S_z = 0$, the orange balls in the black-circle symbolize no magnetic moment is present.

inelastic neutron scattering measurements are required. In summary, single crystals of $\text{BaNd}_2\text{ZnS}_5$ from the BaR_2ZnS_5 family have been successfully synthesized and studied by magnetic bulk measurement and neutron diffraction under magnetic field. Ising magnetic anisotropy of the Nd spins is revealed by the local magnetic susceptibility method with polarized neutrons and their Ising directions are orthogonal to the dimer bonds. Such an arrangement of Ising spins implies symmetric exchange interactions cannot couple the orthogonally arranged dimers. The zero-field magnetic order is a 2- \mathbf{Q} AFM order of FM dimers with Nd spins along their local Ising directions. Two magnetic sublattices with $\mathbf{q}_1 = (\frac{1}{2}, \frac{1}{2}, 0)$ and $\mathbf{q}_2 = (-\frac{1}{2}, \frac{1}{2}, 0)$ constitute the 2- \mathbf{Q} structure and respond to the field along $[1 -1 0]$ differently. The \mathbf{q}_2 magnetic order is suppressed at a critical field, responsible for the kink observed in the magnetization measurement. While the \mathbf{q}_1 magnetic sublattice stays mostly unchanged until 6 T. According to this information, we built the H - T phase diagram from the bulk magnetization and magnetic susceptibility. A critical region was manifested as a spin dimer liquid phase growing out between the stripe phase at lower field and the field polarized phase at upper field. “Spin-flip” and “spin-flop” mechanisms were proposed to explain the formation of the liquid state. Whether the dimer liquid phase could condense at an ultra-low temperature deserves further study. As $\text{BaNd}_2\text{ZnS}_5$ exhibits a unique 2- \mathbf{Q} magnetic square lattice with weak interactions between orthogonal dimers, it can be an exciting candidate to exhibit unique high order symmetries and a potential host for exotic quantum phases. Future dynamic studies including inelastic neutron scattering can provide insight into magnetic interactions and emergent states in the $\text{BaNd}_2\text{ZnS}_5$ SSL and discover interesting dynamic properties of ferromagnetic dimers. An effort in synthesizing large, high quality single crystals is thus called for, as available high-quality single crystals make all these possible.

Methods

Neutron diffraction

To determine the magnetic order single crystal neutron diffraction experiments on the HB-3A DEMAND⁵³ at the High Flux Isotope Reactor at Oak Ridge National Laboratory. A 1.5 mm sample was measured with the two-axis mode down to 1.4 K using a cryomagnet and a wavelength of 1.542 Å from a bent Si-220 monochromator⁵⁴. The measurement was performed with an applied magnetic field of 0, 2 and 6 T parallel to $[1 -1 0]$. The Bilbao Crystallography Server⁵⁵ was used for the magnetic symmetry analysis and Fullprof software⁵⁶ for the magnetic structure refinement. Polarized single crystal neutron diffraction measurements was likewise performed on the HB-3A DEMAND with a polarized neutron beam of 1.542 Å and the calibrated neutron polarization is 72%. The crystal was loaded in a closed-cycle refrigerator with a permanent magnet set providing the fixed field of 0.5 T along $[1 -1 0]$. We measured 17 flipping ratios at 5 K, above T_N . To analyze the resulting flipping ratios the CrysPy software⁵⁷ was used.

Data availability

All relevant data are available from the corresponding author upon reasonable request.

References

- Balents, L. Spin liquids in frustrated magnets. *Nature* **464**, 199–208 (2010).
- Lacroix, C., Mendels, P. & Mila, F. eds. Introduction to Frustrated Magnetism: Materials, Experiments, Theory. vol. 164 (Springer, 2011).
- Smith, R. W. & Keszler, D. A. Synthesis, structure, and properties of the orthoborate $\text{SrCu}_2(\text{BO}_3)_2$. *J. Solid State Chem.* **93**, 430–435 (1991).
- McClarty, P. A. et al. Topological triplon modes and bound states in a Shastry–Sutherland magnet. *Nat. Phys.* **13**, 736–741 (2017).
- Yang, J., Sandvik, A. W. & Wang, L. Quantum criticality and spin liquid phase in the Shastry–Sutherland model. *Phys. Rev. B* **105**, L060409 (2022).
- Dwivedi, V., Hickey, C., Eschmann, T. & Trebst, S. Majorana corner modes in a second-order Kitaev spin liquid. *Phys. Rev. B* **98**, 054432 (2018).
- Eschmann, T., Dwivedi, V., Legg, H. F., Hickey, C. & Trebst, S. Partial flux ordering and thermal Majorana metals in higher-order spin liquids. *Phys. Rev. Res.* **2**, 043159 (2020).
- King, A. D., Nisoli, C., Dahl, E. D., Poulin-Lamarre, G. & Lopez-Bezanilla, A. Qubit spin ice. *Science* **373**, 576–580 (2021).
- Sriram Shastry, B. & Sutherland, B. Exact ground state of a quantum mechanical antiferromagnet. *Phys. B+C.* **108**, 1069–1070 (1981).
- Guo, J. et al. Quantum phases of $\text{SrCu}_2(\text{BO}_3)_2$ from high-pressure thermodynamics. *Phys. Rev. Lett.* **124**, 206602 (2020).
- Corboz, P. & Mila, F. Tensor network study of the Shastry–Sutherland model in zero magnetic field. *Phys. Rev. B* **87**, 115144 (2013).
- Miyahara, S. & Ueda, K. Superstructures at magnetization plateaus in $\text{SrCu}_2(\text{BO}_3)_2$. *Phys. Rev. B* **61**, 3417–3424 (2000).
- Kodama, K. et al. Magnetic superstructure in the two-dimensional quantum antiferromagnet $\text{SrCu}_2(\text{BO}_3)_2$. *Science* **298**, 395–399 (2002).
- Takigawa, M. et al. Incomplete Devil’s Staircase in the Magnetization Curve of $\text{SrCu}_2(\text{BO}_3)_2$. *Phys. Rev. Lett.* **110**, 067210 (2013).
- Jaime, M. et al. Magnetostriction and magnetic texture to 100.75 Tesla in frustrated $\text{SrCu}_2(\text{BO}_3)_2$. *Proc. Natl. Acad. Sci.* **109**, 12404–12407 (2012).
- Sebastian, S. E. et al. Fractalization drives crystalline states in a frustrated spin system. *Proc. Natl. Acad. Sci.* **105**, 20157–20160 (2008).
- Matsuda, Y. et al. Magnetization of $\text{SrCu}_2(\text{BO}_3)_2$ in ultrahigh magnetic fields up to 118 T. *Phys. Rev. Lett.* <https://doi.org/10.1103/PhysRevLett.111.137204> (2013).
- Kageyama, H. et al. Exact dimer ground state and quantized magnetization plateaus in the two-dimensional spin system $\text{SrCu}_2(\text{BO}_3)_2$. *Phys. Rev. Lett.* **82**, 3168–3171 (1999).
- Kodama, K. et al. Field-induced effects of anisotropic magnetic interactions in $\text{SrCu}_2(\text{BO}_3)_2$. *J. Phys.: Condens. Matter* **17**, L61–L68 (2005).
- Zayed, M. E. et al. 4-spin plaquette singlet state in the Shastry–Sutherland compound $\text{SrCu}_2(\text{BO}_3)_2$. *Nat. Phys.* **13**, 962–966 (2017).
- Koga, A. & Kawakami, N. Quantum Phase Transitions in the Shastry–Sutherland Model for $\text{SrCu}_2(\text{BO}_3)_2$. *Phys. Rev. Lett.* **84**, 4461–4464 (2000).
- Berrada, A. et al. Synthèse, cristallogénèse, propriétés magnétiques et effets magnétostrictifs spontanés de quelques tétraborures de terres rares. *Mater. Res. Bull.* **11**, 1519–1526 (1976).
- Siemensmeyer, K. et al. Fractional magnetization plateaus and magnetic order in the Shastry–Sutherland magnet TmB_4 . *Phys. Rev. Lett.* **101**, 177201 (2008).
- Ye, L., Suzuki, T. & Checkelsky, J. G. Electronic transport on the Shastry–Sutherland lattice in Ising-type rare-earth tetraborides. *Phys. Rev. B* **95**, 174405 (2017).
- Ishii, Y. et al. Magnetic properties of the Shastry–Sutherland lattice material $\text{BaNd}_2\text{ZnO}_5$. *Phys. Rev. Mater.* **5**, 064418 (2021).
- Kaduk, J. A., Wong-Ng, W., Greenwood, W., Dillingham, J. & Toby, B. H. Crystal structures and reference powder patterns of BaR_2ZnO_5 ($R = \text{La, Nd, Sm, Eu, Gd, Dy, Ho, Y, Er, and Tm}$). *NIST* **104** 2, (1999).
- Taniguchi, T. et al. Antiferromagnetism of R_2BaPdO_5 ($R = \text{La, Nd, Pr, Sm, Eu, Gd, Dy, Ho}$). *J. Alloy. Compd.* **386**, 63–69 (2005).
- Ishii, Y. et al. High-pressure synthesis, crystal structure, and magnetic properties of the Shastry–Sutherland-lattice oxides $\text{BaLn}_2\text{ZnO}_5$ ($\text{Ln} = \text{Pr, Sm, Eu}$). *J. Solid State Chem.* **289**, 121489 (2020).

29. Zaremba, V. I. et al. Structure and physical properties of RE₂Ge₂In (RE = La, Ce, Pr, Nd). *Solid State Sci.* **6**, 1301–1306 (2004).
30. Tobash, P. H. et al. Crystal growth, structural, and property studies on a family of ternary rare-earth phases RE₂InGe₂ (RE = Sm, Gd, Tb, Dy, Ho, Yb). *Chem. Mater.* **17**, 5567–5573 (2005).
31. Fischer, P. et al. Antiferromagnetic rare-earth ordering in the intermetallic compounds R₂Pd₂In (R = Pr, Nd). *J. Phys.: Condens. Matter* **12**, 7089–7098 (2000).
32. Miiller, W. et al. Magnetic structure of Yb₂Pt₂Pb: ising moments on the Shastry-Sutherland lattice. *Phys. Rev. B* **93**, 104419 (2016).
33. Isaev, L., Ortiz, G. & Dukelsky, J. Local physics of magnetization plateaux in the Shastry-Sutherland model. *Phys. Rev. Lett.* **103**, 177201 (2009).
34. Orendáč, M. et al. Ground state and stability of the fractional plateau phase in metallic Shastry–Sutherland system TmB₄. *Sci. Rep.* **11**, 6835 (2021).
35. Wierschem, K. et al. Origin of modulated phases and magnetic hysteresis in TmB₄. *Phys. Rev. B* **92**, 214433 (2015).
36. Iwakawa, K. et al. Multiple metamagnetic transitions in antiferromagnet Yb₂Pt₂Pb with the Shastry–Sutherland lattice. *J. Phys. Soc. Jpn.* **81**, SB058 (2012).
37. Shimura, Y., Sakakibara, T., Iwakawa, K., Ōnuki, Y. & Sugiyama, K. Magnetization steps in Yb₂Pt₂Pb with the Shastry-Sutherland lattice. *J. Korean Phys. Soc.* **63**, 551–554 (2013).
38. Ochiai, A. et al. Field-induced partially disordered state in Yb₂Pt₂Pb. *J. Phys. Soc. Jpn.* **80**, 123705 (2011).
39. Kim, M. S. & Aronson, M. C. Spin liquids and antiferromagnetic order in the Shastry-Sutherland-lattice compound Yb₂Pt₂Pb. *Phys. Rev. Lett.* **110**, 017201 (2013).
40. Michimura, S., Shigekawa, A., Iga, F., Takabatake, T. & Ohoyama, K. Complex magnetic structures of a Shastry–Sutherland lattice TmB₄ studied by powder neutron diffraction analysis. *J. Phys. Soc. Jpn.* **78**, 024707 (2009).
41. Wakeshima, M. et al. Specific heat and neutron diffraction study on quaternary sulfides BaNd₂CoS₅ and BaNd₂ZnS₅. *J. Solid State Chem.* **174**, 159–164 (2003).
42. Billingsley, B. R., Marshall, M., Shu, Z., Cao, H. & Kong, T. Single crystal synthesis and magnetic properties of a Shastry-Sutherland lattice compound BaNd₂ZnS₅. *Phys. Rev. Mater.* **6**, 104403 (2022).
43. Lhotel, E. et al. Fluctuations and all-in–all-out ordering in dipole-octupole Nd₂Zr₂O₇. *Phys. Rev. Lett.* **115**, 197202 (2015).
44. Cao, H. et al. Ising versus XY anisotropy in frustrated R₂Ti₂O₇ compounds as “seen” by polarized neutrons. *Phys. Rev. Lett.* **103**, 056402 (2009).
45. Cao, H. B., Gukasov, A., Mirebeau, I. & Bonville, P. Anisotropic exchange in frustrated pyrochlore Yb₂Ti₂O₇. *J. Phys. Condens. Matter* **21**, 492202 (2009).
46. Fiebig, M., Fröhlich, D. & Thiele, H.-J. Determination of spin direction in the spin-flop phase of Cr₂O₃. *Phys. Rev. B* **54**, R12681–R12684 (1996).
47. Ding, L. et al. Noncollinear magnetic structure and magnetoelectric coupling in buckled honeycomb Co₄Nb₂O₉: a single-crystal neutron diffraction study. *Phys. Rev. B* **102**, 174443 (2020).
48. Gannon, W. J. et al. Spinon confinement and a sharp longitudinal mode in Yb₂Pt₂Pb in magnetic fields. *Nat. Commun.* **10**, 1123 (2019).
49. Wolter, A. U. B. et al. Field-induced quantum criticality in the Kitaev system alpha-RuCl₃. *Phys. Rev. B* **96**, 041405 (2017).
50. Liang, T. et al. Heat capacity peak at the quantum critical point of the transverse Ising magnet CoNb₂O₆. *Nat. Commun.* **6**, 7611 (2015).
51. Kinross, A. W. et al. Evolution of quantum fluctuations near the quantum critical point of the transverse field Ising chain system CoNb₂O₆. *Phys. Rev. X* **4**, 031008 (2014).
52. Das, D., Gnida, D., Wiśniewski, P. & Kaczorowski, D. Magnetic field-driven quantum criticality in antiferromagnetic CePtIn₄. *Proc. Natl Acad. Sci.* **116**, 20333–20338 (2019).
53. Cao, H. et al. DEMAND, a dimensional extreme magnetic neutron diffractometer at the high flux isotope reactor. *Crystals* **9**, 5 (2019).
54. Chakoumakos, B. C. et al. Four-circle single-crystal neutron diffractometer at the High Flux Isotope Reactor. *J. Appl. Cryst.* **44**, 655–658 (2011).
55. Perez-Mato, J. M. et al. Symmetry-based computational tools for magnetic crystallography. *Annu. Rev. Mater. Res.* **45**, 217–248 (2015).
56. Rodríguez-Carvajal, J. Recent advances in magnetic structure determination by neutron powder diffraction. *Phys. B: Condens. Matter* **192**, 55–69 (1993).
57. Kibalin, I. A. & Gukasov, A. Local magnetic anisotropy by polarized neutron powder diffraction: Application of magnetically induced preferred crystallite orientation. *Phys. Rev. Res.* **1**, 033100. <https://github.com/ikibalin/cryspy> (2019).

Acknowledgements

The research at Oak Ridge National Laboratory (ORNL) was supported by the U.S. Department of Energy (DOE), Office of Science, Office of Basic Energy Sciences, Early Career Research Program Award KC0402020, under Contract DE-AC05-00OR22725. This research used resources at the High Flux Isotope Reactor, a DOE Office of Science User Facility operated by ORNL. We acknowledge and thank Zachary Morgan for the assistance with the data reduction of the neutron diffraction experiments. We acknowledge and thank Cristian Batista for the helpful discussions. We thank Chenyang Jiang for the assistance with the experimental polarized neutron diffraction.

Author contributions

H.C. cultivated the research; B.R.B. and T.K. synthesized single-crystal samples and performed magnetization measurements; M.M. and H.C. performed neutron scattering experiments and analyze the data; X.B. assisted with polarized neutron data analysis; X.B. and Q.M. contributed to theoretical discussion; M.M. and H.C. wrote manuscript with comments from all authors.

Competing interests

The authors declare no competing interests. This manuscript has been authored by UT-Battelle, LLC under Contract No. DE-AC05-00OR22725 with the U.S. Department of Energy. The United States Government retains and the publisher, by accepting the article for publication, acknowledges that the United States Government retains a non-exclusive, paid-up, irrevocable, world-wide license to publish or reproduce the published form of this manuscript, or allow others to do so, for United States Government purposes. The Department of Energy will provide public access to these results of federally sponsored research in accordance with the DOE Public Access Plan (<http://energy.gov/downloads/doepublic-access-plan>).

Additional information

Supplementary information The online version contains supplementary material available at <https://doi.org/10.1038/s41467-023-39409-1>.

Correspondence and requests for materials should be addressed to Huibo Cao.

Peer review information *Nature Communications* thanks the anonymous reviewer(s) for their contribution to the peer review of this work.

Reprints and permissions information is available at <http://www.nature.com/reprints>

Publisher's note Springer Nature remains neutral with regard to jurisdictional claims in published maps and institutional affiliations.

Open Access This article is licensed under a Creative Commons Attribution 4.0 International License, which permits use, sharing, adaptation, distribution and reproduction in any medium or format, as long as you give appropriate credit to the original author(s) and the source, provide a link to the Creative Commons license, and indicate if changes were made. The images or other third party material in this article are included in the article's Creative Commons license, unless indicated otherwise in a credit line to the material. If material is not included in the article's Creative Commons license and your intended use is not permitted by statutory regulation or exceeds the permitted use, you will need to obtain permission directly from the copyright holder. To view a copy of this license, visit <http://creativecommons.org/licenses/by/4.0/>.

© The Author(s) 2023